Materials Transactions, Vol. 49, No. 6 (2008) pp. 1385 to 1394

Preparation of Zr-Based Metallic Glass Wires for Biomaterials by Arc-Melting Type Melt-Extraction Method

Takeshi Nagase[1], Koichi Kinoshita[2] and Yukichi Umakoshi[1,*]

[1]*Division of Materials and Manufacturing Science, Graduate School of Engineering, Osaka University, Suita 565-0871, Japan*
[2]*Department of Mechanical Science and Bioengineering, Graduate School of Engineering Science, Osaka University, Toyonaka 560-8531, Japan*

New Zr-based metallic glass wires with and without bio-toxic elements of Ni and Al for the application to biomaterials were prepared by arc-melting type melt-extraction method and their characteristics were tested. The continuous metallic glass wires with a good white luster and smooth surface were obtained in various alloys such as conventional Zr-Al-Ni-Cu, Ni-free Zr-Al-Co-Cu, and Ni and Al free Zr-Ti-Co alloys. The Zr-based metallic glass wires exhibit high tensile strength reaching 1 GPa. Furthermore, the metallic glass wires showed good bending ductility and could be bent through 180 degrees without fracture. The Zr-based metallic glass wires achieve simultaneously high tensile strength, good bending ductility and high thermal stability. [doi:10.2320/matertrans.MRA2008006]

(Received January 8, 2008; Accepted March 5, 2008; Published April 16, 2008)

Keywords: *metallic glass, amorphous, wire, fiber, zirconium-based alloy, melt-extraction method, bio material*

1. Introduction

Metallic amorphous alloys are known to show superior mechanical properties such as high tensile strength, low Young's modulus and large elastic elongation limit of about 2%.[1,2] Wire shape samples with a circular cross section are favorable for the utilization of the superior mechanical strength. The amorphous alloy wires with diameters of the order of 100 μm are obtained in Fe-Si-B,[3,4] Fe-Si-B-M (M = Nb, Ta, Cr or Mo),[3,4] Fe-P-C,[4,5] Fe-P-C-M (M = Nb, Ta, Cr or Mo),[4,5] Fe-Ni-Si-B,[4] Fe-Ni-P-C,[4] Co-Si-B,[6] Co-Cr-P-B-Be,[7] Co-Fe-Cr-P-B-Be,[7] Ni-Si-B-Al,[8] Pd-Cu-Si,[9] Pd-Ni-P[10] and Pt-Ni-P[10] by in rotating-liquid melt-spinning method.[11] Some Fe-based and Co-based amorphous alloys such as Fe-Co-Cr-Si-B have been used in various application fields by utilizing their superior mechanical properties, high corrosion resistance and unique soft magnetic properties.[12,13] However, liquid mediums must be used in the in-rotating-liquid melt spinning method. In this method, formation of Al-, Mg-, Ti- and Zr- based amorphous alloy wires has not been reported to date because of the high reactivity between these molten alloys and the liquid coolants. The melt-extraction method without any cooling medium is expected to produce continuous amorphous wires with high reactivity in molten state.[14,15] The preparation of amorphous wires not only in conventional Fe-Si-B[16] and Co-Si-B[16] amorphous alloys but also in Al-Ni-Ce,[17,18] Cu-Ti-Zr,[18] Zr-Al-Cu,[19] Zr-Al-Ni-Cu[19] and Zr-Ti-Al-Ni-Cu[19] alloys was reported by the melt-extraction method. Among the above described amorphous wires, Zr-based alloy wires are of great interest as a candidate for biomaterials because of their unique mechanical properties and high glass forming ability.

Table 1 shows the amorphous alloy systems investigated for biomedical applications: various Zr-based alloys such as traditional Vitreloy as well as newly developed alloys of Bio-1 and Ni-free BAM-11 have been investigated. However, all alloys listed in Table 1 have not continuous wire shape with circular cross section but other one such as thin film coating, melt-spun specimen or as-cast bulk samples. Moreover, one can notice that the previous alloys contain toxic elements such as Ni and Al for biomedical application.

The first aim of this paper is to prepare Zr-based amorphous wire not only of conventional Zr-Al-Ni-Cu and Zr-Ti-Al-Ni-Cu alloys but also of new alloys without any toxic elements by arc-melting type melt-extraction method.[19] The second is to investigate the shape, structure, thermal stability and mechanical properties of melt-extracted wires.

2. Experimental Procedure

2.1 Alloy system

Referring to the previous research works about Zr-based metallic glass for biomedical applications, $Zr_{57}Nb_5Al_{10}Ni_{12.6}Cu_{15.4}$ (Vit-106), $Zr_{52.5}Ti_5Al_{10}Ni_{14.6}Cu_{17.9}$ (Vit-105/BAM-11), $Zr_{55}Ti_{5.2}Al_{10.5}Ni_{13.2}Cu_{16.1}$ (Zr-Ti-Al-Ni-Cu) and $Zr_{52.5}Ti_5Al_{10}Cu_{32.5}$ (Ni free BAM-11) alloys were investigated. These quinary and quaternary alloys contain toxic elements of Ni and Al. Ni-free and Al-free alloys were developed from $Zr_{65}Al_{7.5}Ni_{10}Cu_{17.5}$ (Zr-Al-Ni-Cu) alloy by replacing Ni with Co and Al with Ti; $Zr_{65}Al_{7.5}Co_{10}Cu_{17.5}$ (Zr-Al-Co-Cu), $Zr_{65}Al_{7.5}Co_{27.5}$ (Zr-Al-Co) and $Zr_{65}Ti_{7.5}Co_{27.5}$ (Zr-Ti-Co). Binary $Zr_{60}Ti_{40}$ (Zr-Ti) alloy was also investigated to compare the Zr-based amorphous alloy systems and conventional crystalline alloy system. The alloys investigated in the present study are listed in Table 1. The compositions are expressed in nominal atomic per cent.

2.2 Experimental procedure

Master ingots of Zr-based alloys were prepared by arc-melting a mixture of pure Zr, Ti, Co, Cu, Ni and Al (purity > 99.9%) by arc melting under highly purified Ar atmosphere. The rapidly solidified wires were prepared by arc melting type melt extraction method. Figure 1 shows the schematic illustration (a) and photograph (b) of the apparatus

*Corresponding author, E-mail: umakoshi@mat.eng.osaka-u.ac.jp

Table 1 Various amorphous alloys and metallic glasses investigated for bio-materials.

Alloy-system	Alloy composition	(Alloy name)	Reference	Present study
Co-P	$Co_{80}P_{20}$		20, 21)	
Co-Cr-C	—		20)	
Co-Si-B	—		22, 23)	
Co-Fe-Si-B	—		22)	
Co-Fe-Nb-Si-B	—		22, 23)	
Co-Zr	$Co_{90}Zr_{10}$		24)	
Co-Zr	$Co_{53}Zr_{47}$		24)	
Co-Zr-B	$Co_{80}Zr_{10}B_{10}$		24)	
Co-Zr-B-Al	$Co_{75}Zr_{10}B_{10}Al_5$		24)	
Co-Zr-B-Ti	$Co_{75}Zr_{10}B_{10}Ti_5$		24)	
Co-Ti-B	$Co_{65}Ti_{25}B_{10}$		24)	
Co-Ti-B-Si	$Co_{60}Ti_{25}B_{10}Si_5$		24)	
Fe-Cr-Si-B	—		22, 23)	
Fe-Cr-P-C	$Fe_{66}Cr_{14}P_{13}C_7$		23)	
Pd-Si-Cr	$Pd_{78}Si_{16}Cr_6$		25, 26)	
Pd-Si-Cu	$Pd_{78}Si_{16}Cu_6$		25, 26)	
Pd-Si-Cr-Cu	$Pd_{78}Si_{16}Cr_xCu_{6-x}$ (x = 2–4)		25, 26)	
Pd-Ni-Cu-P	$Pd_{40}Ni_{10}Cu_{30}P_{20}$		27)	
Ti-In-Cu	—		28)	
Ti-Si-Cu	—		28)	
Ti-Ta-Zr-Si	$(Ti_xTa_yZr_z)_{85}Si_{15}$ (x = 60–80, y = 5–20, z = 5–20)		29)	
Zr-Nb-Al-Ni-Cu	$Zr_{58.5}Nb_{2.8}Al_{10.3}Ni_{12.8}Cu_{15.6}$	(Vit-106a)	30)	
	$Zr_{57}Nb_5Al_{10}Ni_{12.6}Cu_{15.4}$	(Vit-106)	Present study	○
Zr-Ti-Al-Ni-Cu	$Zr_{52.5}Ti_5Al_{10}Ni_{14.6}Cu_{17.9}$	(Vit-105, BAM-11)	31)	○
	$Zr_{55}Ti_{5.2}Al_{10.5}Ni_{13.2}Cu_{16.1}$		Present study	○
Zr-Ti-Al-Cu	$Zr_{52.5}Ti_5Al_{10}Cu_{32.5}$	(Ni free BAM-11)	31)	○
Zr-Al-Co-Cu	$Zr_{55}Al_{10}Co_5Cu_{30}$		32)	
	$Zr_{65}Al_{7.5}Co_{10}Cu_{17.5}$		Present study	○
Zr-Al-Fe-Cu	$Zr_{58}Cu_{22}Fe_8Al_{12}$	(Bio-1)	30)	
	$Zr_{60}Cu_{20}Fe_5Al_{10}$		33)	
Zr-Al-Ni-Cu	$Zr_{65.0}Al_{7.5}Ni_{10}Cu_{17.5}$		26, 34, 35)	○
	$Zr_{65}Al_{10}Ni_{10}Cu_{15}$		26)	
Zr-Co-B-Al	$Zr_{47}Co_{38}B_{10}Al_5$		36)	
Zr-Co-B-Si	$Zr_{47}Co_{38}B_{10}Si_5$		36)	
Zr-Al-Co	$Zr_{55}Al_{20}Co_{25}$		33)	
	$Zr_{65}Al_{7.5}Co_{27.5}$		Present study	○
Zr-Al-Cu	$Zr_{65}Al_{7.5}Cu_{27.5}$		34)	
Zr-Ti-Co	$Zr_{65}Ti_{7.5}Co_{27.5}$		Present study	○
Zr-Co	$Zr_{78.5}Co_{21.5}$		25)	

(NISSIN-GIKEN, NEV-AT3). The edge angle of Cu roll with the diameter of 200 mm was fixed to 60 degrees. The rotation speed was fixed at 33.3 turns s^{-1} (2000 r.p.m) and circumferential velocity of Cu roll is 21 ms^{-1}. The molten pool of mother alloy was maintained on a water cooled copper mold during extraction under Ar atmosphere. In this apparatus, the position of Cu roll can be controlled. The extraction of molten mother alloy was performed by moving down of the rotating Cu roll. In the present study, conventional melt-spun ribbon was also prepared by single roller melt-spinning method in Ar atmosphere to compare the structure and thermal stability between melt-spun ribbons and melt-extracted wires. The formation of an amorphous phase was confirmed by X-ray diffraction (XRD) using Cu-Kα radiation and differential scanning calorimetry (DSC) at a heating rate of 0.67 Ks^{-1}. The surface morphology was examined by optical microscopy (OM) and scanning electron microscopy (SEM). Tensile strength of the wire specimens was measured by an Instron-type testing machine at a strain rate of 4.2×10^{-4} s^{-1} in the air. Ductility was evaluated by a simple bending test. Ductile wire means that the wire can be bend through 180 degrees without fracture.

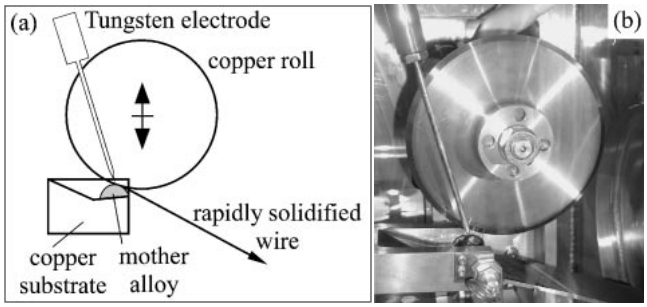

Fig. 1 Schematic Illustration of Arc-melt type melt-extraction machine used in the present study. (a) schematic illustration of the method, (b) photograph of machine.

3. Results

3.1 Morphology of melt-extracted wires

Figure 2 shows typical examples of outer appearance of the wires prepared by arc-melting type melt-extraction method in Zr-based alloys; (a) Zr-Al-Ni-Cu, (b) Zr-Al-Co, (c) Zr-Ti-Co, and (d) Zr-Ti. The continuous metallic wires can be obtained not only in conventional Zr-Al-Ni-Cu alloy but also in Zr-Al-Co, Zr-Ti-Co and Zr-Ti alloys without any harmful elements of Ni, Al and Be from the viewpoint of biocompatibility. Melt-extracted wire shows metallic white luster color, which is similar to the conventional metallic crystalline wires prepared by wire-drawing process.

Figure 3 shows typical examples of outer surface appearance of Zr-based alloy wires, together with that of conventional Fe-based crystalline wire prepared by wire-drawing process. Melt-extracted Zr-Al-Ni-Cu ((a) and (e)) and Zr-Ti-Co ((b) and (f)) wires have a smooth surface and no distinct ruggedness. The wires show the uniformity in diameter with negligible fluctuation. In contrast, melt-extracted Zr-Ti ((c) and (g)) and conventional Fe-based alloy ((d) and (h)) wires do not show a smooth surface but slight ruggedness. To investigate surface morphology of melt-extracted wires in detail, SEM observation was performed. The obtained results are shown in Fig. 4. The superior specularity surface without any ruggedness can be confirmed not only by OM observation but also by SEM observation in melt-extracted Zr-Al-Ni-Cu ((a) and (e)) and Zr-Ti-Co ((b) and (f)) wires. No significant change of contrast corresponding to crystalline precipitates was seen, indicating that Zr-Al-Ni-Cu and Zr-Ti-Co alloys can be produced in the form of almost all

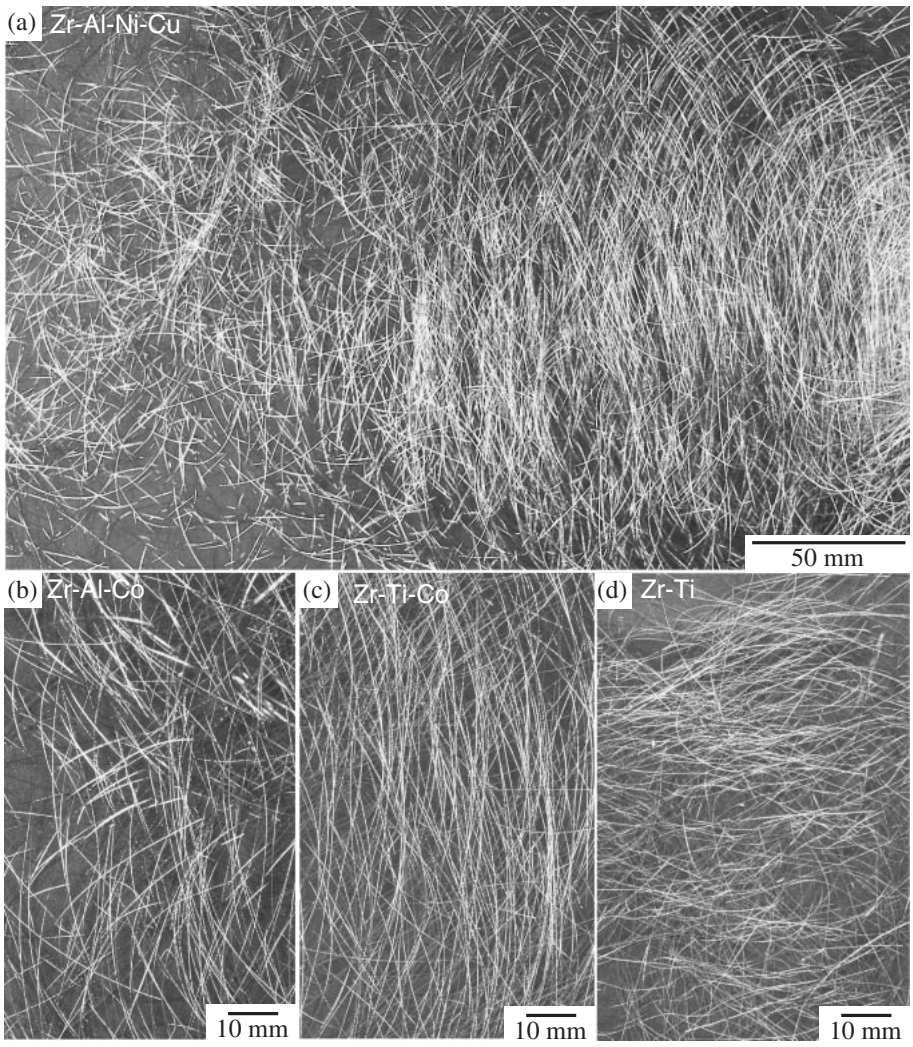

Fig. 2 Outer appearance of melt-extracted Zr-based alloy wires; (a) $Zr_{65}Al_{7.5}Ni_{10}Cu_{17.5}$, (b) Ni free type $Zr_{65}Al_{7.5}Co_{27.5}$, (c) Ni and Al free type $Zr_{65}Ti_{7.5}Co_{27.5}$, and (d) $Zr_{80}Ti_{20}$.

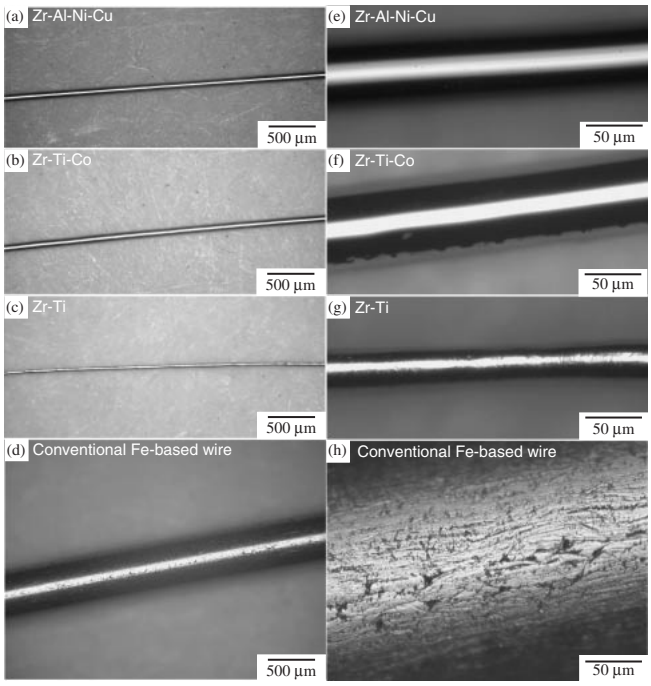

Fig. 3 Outer surface appearance of melt-extracted Zr-based alloy wires and conventional Fe-based crystalline wire prepared by wire-drawing process; (a) $Zr_{65}Al_{7.5}Ni_{10}Cu_{17.5}$, (b) Ni and Al free type $Zr_{65}Al_{7.5}Co_{27.5}$, (c) $Zr_{80}Ti_{20}$, and (d) conventional Fe-based crystalline wire.

amorphous single phase wires. Formation of amorphous phase was confirmed by XRD and DSC measurements as mentioned in the later. Melt-extracted Zr-Ti (c) shows fluctuation in the diameter, which is different from Zr-Al-Ni-Cu (a) and Zr-Ti-Co (b). The contrast corresponding to crystalline precipitation was seen in close-up image (g) in Zr-Ti alloy. The crystallization of extracted melt occurs in Zr-Ti alloy, resulting in inducing ruggedness in the surface and fluctuation in the diameter. In conventional Fe-based wires prepared by wire-drawing process ((d) and (h)), the trace of metallic flow along the die can be confirmed. The surface ruggedness in wires sometimes acts as an origin of the destruction for a surface crack. The melt-extraction method is very effective for obtaining metallic amorphous wires with superior smooth surface which is not realized by conventional metal plastic forming process.

Figure 5 shows the schematic illustration to evaluate the degree of circularity in the cross section of the wire (roundness, ε) (a) and typical examples of optical micrographs of the transverse cross sections of melt-extracted wires ((b) and (c)). The diameter and shape of cross section are very sensitive to the melt-extraction conditions such as the edge shape of the Cu roll, circumferential velocity of Cu roll, temperature of molten metal and so on. In the present study, the diameter and the roundness of Zr-Ti-Al-Ni-Cu, Zr-Al-Ni-Cu, Zr-Ti-Al-Cu, Zr-Al-Co-Cu, Zr-Al-Co and Zr-Ti-Co wires were evaluated, and it was found no significant ruggedness on the surface and fluctuation of the diameter in the 8 alloy wires. The diameter and roundness of their wires are summarized in Table 2, together with data of Zr-Ti alloy and conventional Fe-based alloy wires. In Zr-Ti alloy wire, data obtained at various positions were listed because of the fluctuation of the diameter. The diameter of quinary, quaternary and ternary Zr-based alloy wires was about 100 μm; Zr-Al-Ni-Cu(b) and Zr-Ti-Co(c) wires showed the minimum and maximum diameter among quinary, quaternary and ternary Zr-based alloys listed in Table 2, respectively. Their wires have circular cross sections shown in Fig. 5(b) and (c) and no irregular contrast corresponding to the precipitation of crystalline phase. Similar circular cross section images also can be seen in Zr-Ti-Al-Ni-Cu, Zr-Ti-Al-Cu, Zr-Al-Co-Cu and Zr-Al-Co wires, and the roundness of quinary, quaternary and ternary Zr-based alloy wires listed in Table 2 is over 95. The features of morphology such as no ruggedness on outer surface, no fluctuation in the diameter and circular cross section image in melt-extracted Zr-based wires indicate that melt-extraction method is very effective for preparing metallic wires in alloy systems containing reactive metals as a main component.

3.2 Amorphous phase formation in melt-extracted wires

To confirm the formation of an amorphous phase in melt-extracted wires, XRD analysis and DSC measurement were performed. Figure 6 shows XRD patterns of melt-extracted Zr-based alloy wires; (a) quinary alloys, (b) quaternary alloys, (c) ternary alloys and (d) binary alloy. The XRD patterns in quinary Zr-Ti-Al-Ni-Cu alloys in Fig. 6(a), and quaternary Zr-Al-Ni-Cu, Zr-Al-Co-Cu and Zr-Ti-Al-Cu alloys in Fig. 6(b) show only a broad peak whose peak position is around 37 degree. These results indicate that melt-extracted wires consist of an amorphous single phase and they are in agreement with the results of outer surface and cross section observation by OM and SEM shown in Figs. 2, 3 and 4. In ternary Zr-Al-Co and Zr-Ti-Co alloys in Fig. 6(c), not only broad peak but also sharp diffraction peaks corresponding to crystalline phases can be seen. Crystalline precipitates exist in ternary amorphous wires. The quantity of crystalline precipitates is very small because very weak intensity in XRD pattern and no significant contrast corresponding crystalline precipitates on the outer surface and cross section observation by OM and SEM. Zr-Ti melt extracted wire shows only sharp diffraction peaks corresponding to α-Zr phase with h.c.p. structure. Amorphous phase was not formed in Zr-Ti alloy.

Figure 7 shows XRD patterns of Zr-based alloy melt-extracted wires and melt-spun ribbons prepared by conventional single-roller melt-spinning method. In the figure, Ribbon(Free) and Ribbon(Roll side) mean data obtained on the free surface and the roll-side surface of the melt-spun ribbon, respectively. $Zr_{65}Al_{7.5}Ni_{10}Cu_{17.5}$ alloy has extremely high glass forming ability (GFA). Only broad peak can be seen in Fig. 7(a) for both wire and ribbon. No significant difference in XRD pattern between wire and ribbon was detected. In contrast, the XRD patterns of wires of ternary $Zr_{65}Al_{7.5}Co_{27.5}$ in Fig. 7(b) and $Zr_{65}Ti_{7.5}Co_{27.5}$ in Fig. 7(c) alloys show sharp diffraction peaks corresponding to crystalline precipitates together with a broad peak. These results indicate that glass forming tendency of melt-extraction process in the ternary alloys is slightly lower than that of conventional single roller melt spinning process, which is similar to the previous work of Zr-Al-Cu alloy reported by Kimura *et al.*[19] The difference in constituent phases between

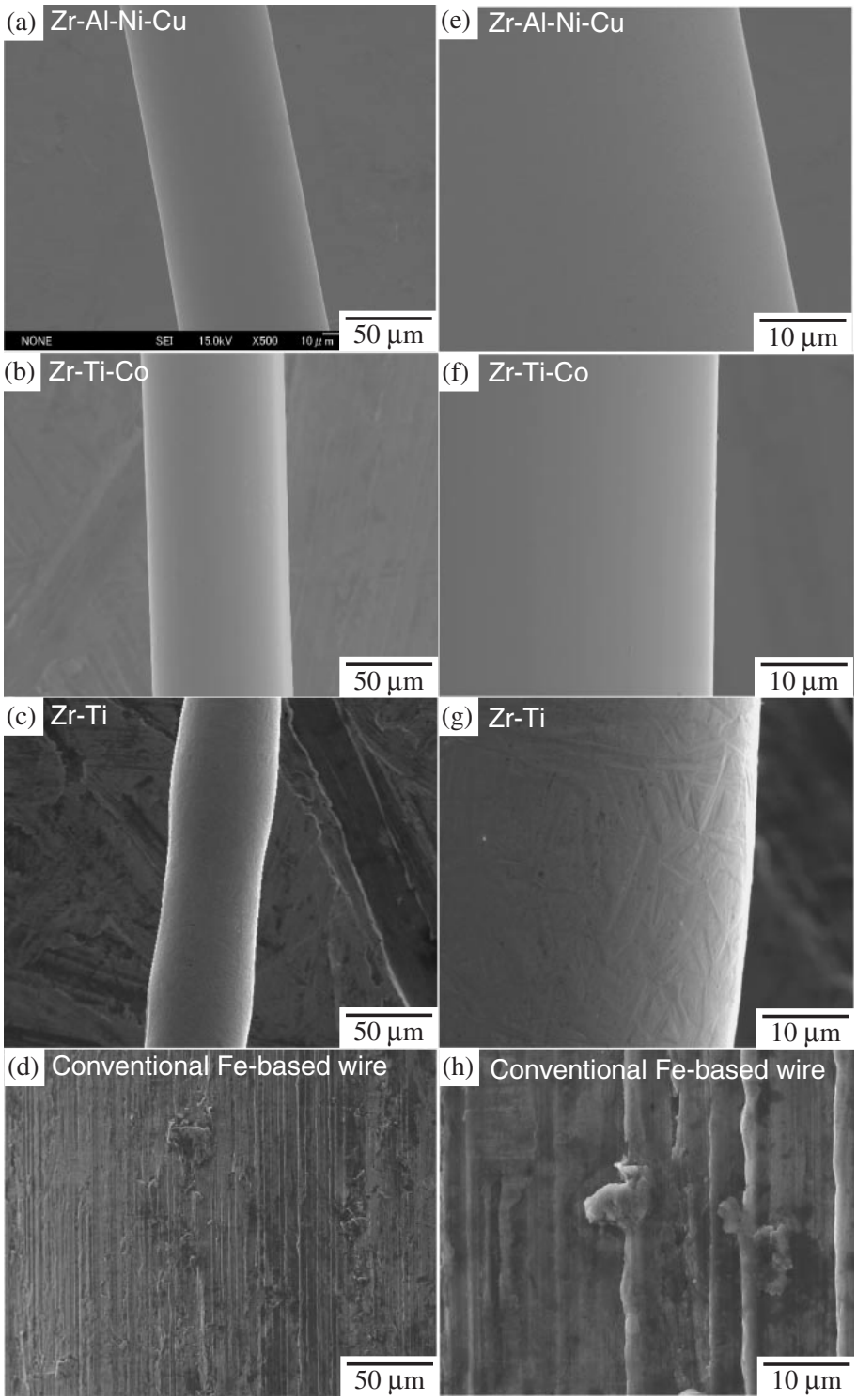

Fig. 4 SEM images of melt-extracted Zr-based alloy wires and conventional Fe-based crystalline wire prepared by wire-drawing process; (a) and (e) $Zr_{65}Al_{7.5}Ni_{10}Cu_{17.5}$, (b) and (f) Ni and Al free type $Zr_{65}Al_{7.5}Co_{27.5}$, (c) and (g) $Zr_{80}Ti_{20}$, and (d) and (h) conventional Fe-based crystalline wire. (e), (f), (g) and (h) are close-up images of (a), (b), (c) and (d), respectively.

melt-extraction method and single roller melt-spinning method may be due to the difference in the circumferential velocity of Cu roll in the present study; 21 ms^{-1} (2000 r.p.m.) in melt-extraction method and 42 ms^{-1} (4000 r.p.m.) in single roller melt-spinning method. Modification of the melt-extraction apparatus and optimization of the condition is important to obtain an amorphous single phase wire in Zr-based alloys.

Thermal properties and thermal stability were examined by DSC measurement at a heating rate of 0.67 Ks^{-1}. The DSC curves are shown in Figs. 8 and 9. Figure 8 shows DSC curves of melt-extracted Zr-based alloy wires; (a) quinary alloys, (b) quaternary alloys, (c) ternary alloys and (d) binary alloy. The DSC curve in of quinary Zr-Ti-Al-Ni-Cu alloys (a), quaternary Zr-Al-Ni-Cu, Zr-Al-Co-Cu and Zr-Ti-Al-Cu alloys show an anomalous endothermic reaction

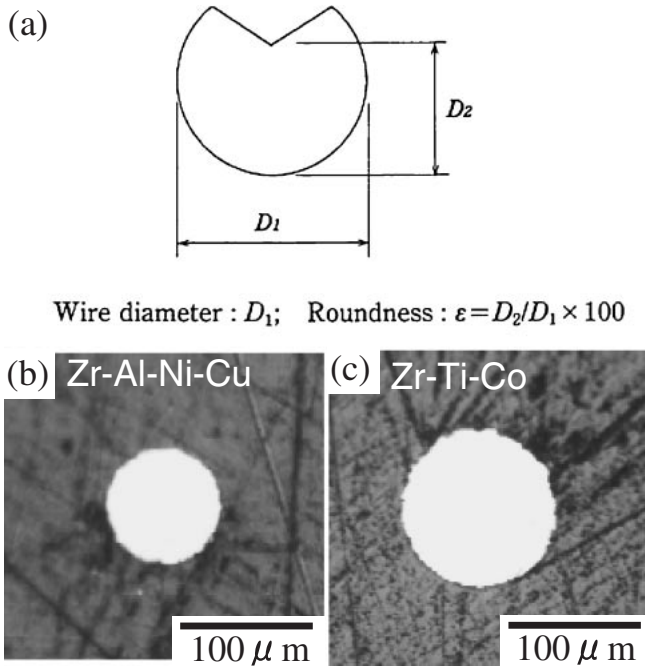

Fig. 5 Schematic illustration showing the definition of the degree of circular in cross section of the wire (a) and typical examples of cross section shape in melt-extracted Zr-based alloy wires (b) and (c); (b) $Zr_{65}Al_{7.5}Ni_{10}Cu_{17.5}$, (c) Ni and Al free type $Zr_{65}Ti_{7.5}Co_{27.5}$.

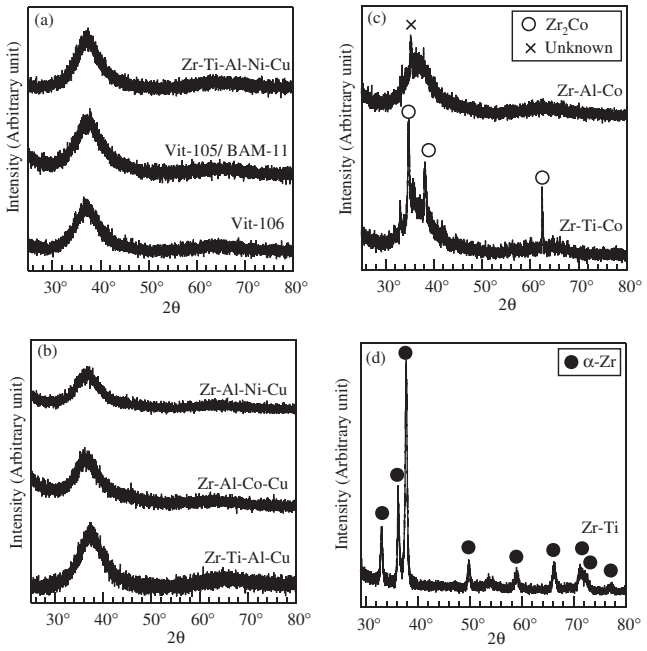

Fig. 6 X-ray diffraction patterns of melt-extracted Zr-based alloy wires; (a) 5 component alloys, (b) 4 component alloys, (c) ternary alloys and (d) binary alloy.

Table 2 Diameter and degree of circularity of melt-extracted Zr-based alloy wires and conventional Fe-based crystalline wire.

Alloy-system	Alloy composition	(Alloy name)	$d1$ [μm]	$d2$ [μm]	ε
Zr-Nb-Al-Ni-Cu	$Zr_{57}Nb_5Al_{10}Ni_{12.6}Cu_{15.4}$	(Vit-106)	108	107	99
Zr-Ti-Al-Ni-Cu	$Zr_{52.5}Ti_5Al_{10}Ni_{14.6}Cu_{17.9}$	(Vit-105, BAM-11)	104	100	97
	$Zr_{55}Ti_{5.2}Al_{10.5}Ni_{13.2}Cu_{16.1}$		101	96	95
Zr-Ti-Al-Cu	$Zr_{52.5}Ti_5Al_{10}Cu_{32.5}$	(Ni free BAM-11)	100	96	96
Zr-Al-Co-Cu	$Zr_{65}Al_{7.5}Co_{10}Cu_{17.5}$		88	84	95
Zr-Al-Ni-Cu	$Zr_{65.0}Al_{7.5}Ni_{10}Cu_{17.5}$		88	84	95
Zr-Al-Co	$Zr_{65}Al_{7.5}Co_{27.5}$		112	108	97
Zr-Ti-Co	$Zr_{65}Ti_{7.5}Co_{27.5}$		123	118	96
Zr-Ti	$Zr_{60}Ti_{40}$		135	92	68
			111	93	83
			95	67	70
Fe-based alloy (Conventional Fe-based crystalline alloy wire)			300	300	100

indicated by T_g and sharp exothermic peaks corresponding to thermal crystallization. The anomalous endothermic reaction corresponds to the glass-to-liquid transition. Ternary Zr-Al-Co and Zr-Ti-Co alloys show only sharp exothermic peaks, and supercooled liquid region can not be detected in Fig. 8(c). This indicates that GFA of the ternary alloys is lower than that in the quinary and quaternary alloys. The difference in GFA among these alloys is in good agreement with the constituent phases in melt-extraction wires; an amorphous single phase wires can be obtained only in the quinary and quaternary alloys. Figure 8(d) shows DSC curve of binary Zr-Ti crystalline wire, together with that of Zr-Al-Ni-Cu amorphous wire for comparison. Zr-Ti crystalline wire shows an endothermic reaction indexed by A at the temperature about 880 K. This is due to the phase transition from α-phase with h.c.p. structure to β-phase with b.c.c. structure, which is in good agreement with equilibrium phase diagram. Amorphous state could not be obtained in this wire.

Figure 9 shows typical examples of difference in DSC curves between melt-extracted wire and melt-spun ribbon of Zr-based alloys. The DSC curves of $Zr_{65}Al_{7.5}Ni_{10}Cu_{17.5}$ alloy with extremely high GFA illustrated in Fig. 9(a) shows no distinct difference in DSC curves such as the glass transition temperature, crystallization temperature, crystallization enthalpy, and shape of crystallization exothermic peaks. The crystallization enthalpy of DSC curve of ternary Zr-Ti-Co

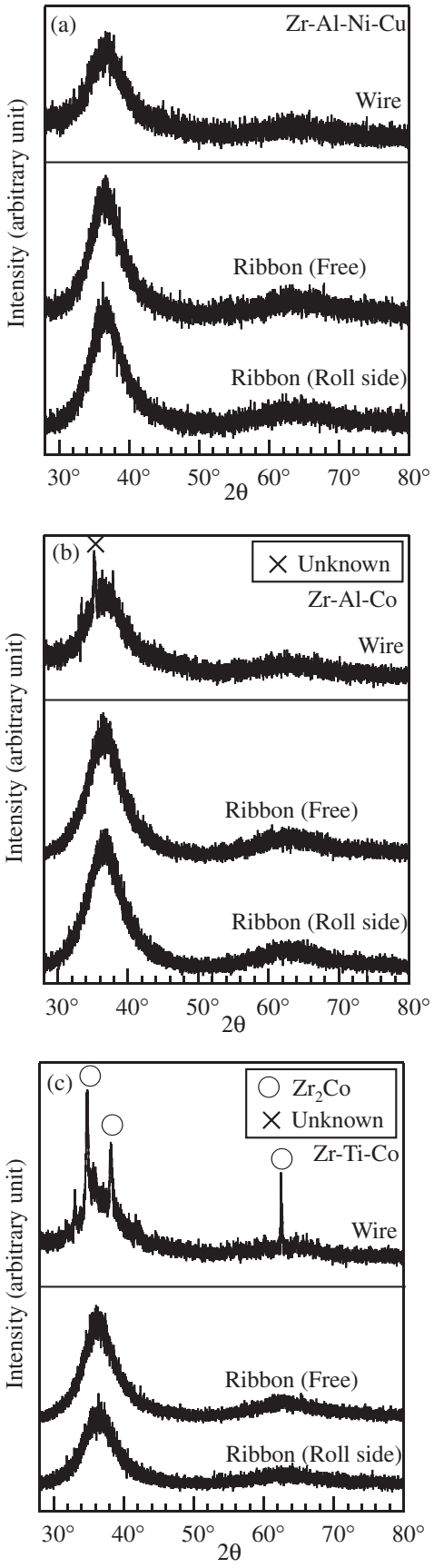

Fig. 7 X-ray diffraction patterns of melt-extracted wires and melt-spun ribbons prepared by conventional single-roller melt-spinning method in Zr-based alloys. Ribbon(Free) and Ribbon(Roll side) mean the XRD patterns obtained by the free surface and that by the roll-side in melt-spun ribbon, respectively; (a) $Zr_{65}Al_{7.5}Ni_{10}Cu_{17.5}$, (b) Ni free type $Zr_{65}Al_{7.5}Co_{27.5}$, and (c) Ni and Al free type $Zr_{65}Ti_{7.5}Co_{27.5}$.

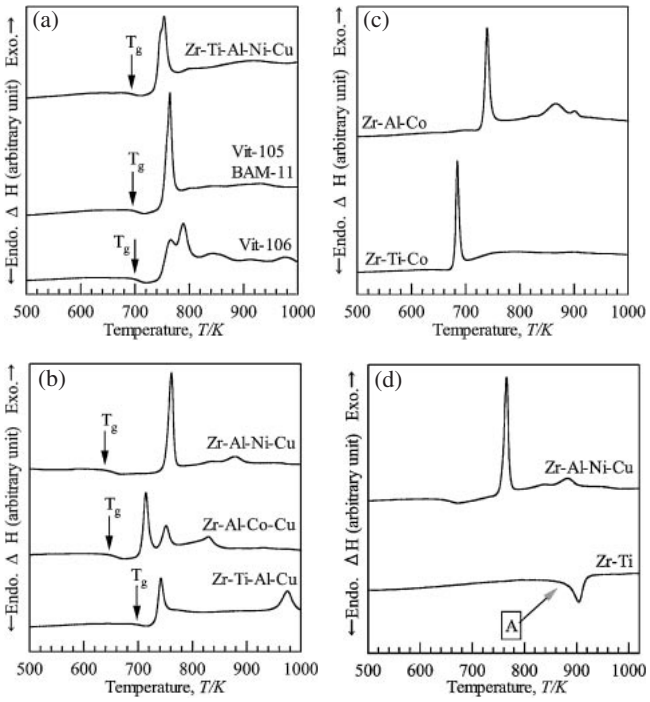

Fig. 8 DSC curves of melt-extracted Zr-based alloy wires at a heating rate of 0.67 Ks^{-1}; (a) quinary alloys, (b) quaternary alloys, (c) ternary alloys and (d) binary alloy.

alloy wire shown in Fig. 9(b) is slightly smaller than that of melt-spun ribbon because it contains crystalline phase. But one should notice that the DSC curves of both alloy wires are almost similar to those of melt-spun amorphous ribbons. The DSC curves indicate that there is no significant difference in thermal properties of amorphous phase between the melt-extracted wires and melt-spun ribbons.

3.3 Mechanical properties of melt-extracted wires

Mechanical properties of melt-extracted Zr-based metallic glass wires were investigated by the tensile test in the air. Figure 10 shows typical examples of tensile stress-elongation curves of melt-extracted Zr-based metallic glass wires of $Zr_{65}Al_{7.5}Ni_{10}Cu_{17.5}$ alloy. Metallic glass wire shows high tensile fracture strength (σ_f) reaching more than 1 GPa. The fluctuation of σ_f is very large because of the experimental artifacts based on difficulty of chucking the wire whose diameter is about 100 μm. The σ_f of melt-extracted wire was evaluated by the trimmed mean of measured σ_f values of more than 7 samples. The average σ_f value is listed in Table 3. Average σ_f of metallic glass of Zr-Ti-Al-Ni-Cu, Zr-Al-Ni-Cu, Zr-Ti-Al-Cu, Zr-Al-Co-Cu and Zr-Al-Co alloys was over 1 GPa, and it is strong enough for biomedical applications. No distinct plastic elongation is seen in the tensile stress-elongation curves, which is similar to the conventional melt-spun amorphous ribbon but different from conventional crystalline wires. Although the distinct plastic elongation cannot be obtained, metallic glass wire shows large tensile elongations (l_f) reaching 2% because of the large elastic elongation limit. In the present study, the elongation of wires was measured not by the strain gage but by the position of the crosshead. The value of l_f listed in Table 3 is, therefore slightly higher than those of the

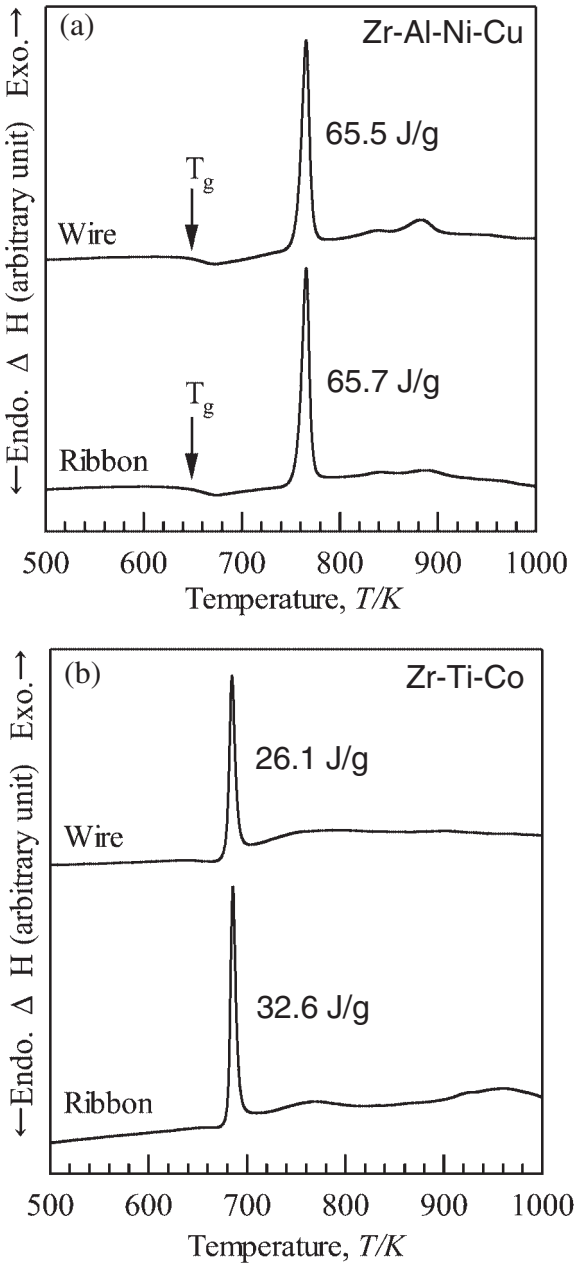

Fig. 9 Difference in DSC curves between melt-extracted wires and melt-spun ribbons prepared by conventional single-roller melt-spinning method in Zr-based alloys: (a) $Zr_{65}Al_{7.5}Ni_{10}Cu_{17.5}$ and (b) $Zr_{65}Ti_{7.5}Co_{27.5}$.

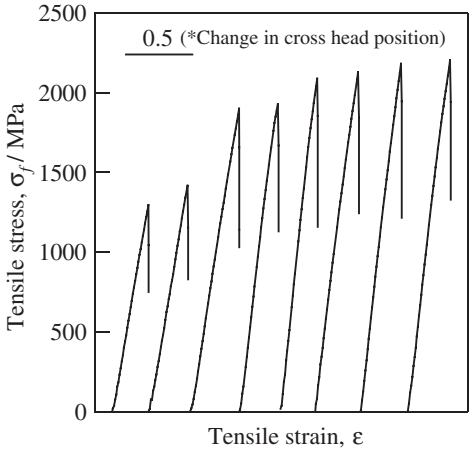

(*) the elongation of wires was measured not by the strain gage but by displacement of the crosshead position.

Fig. 10 Tensile stress-elongation curves of melt-extracted Zr-based wires in $Zr_{65}Al_{7.5}Ni_{10}Cu_{17.5}$ alloy. (*) the elongation of wires was measured not by the strain gage but by displacement of the crosshead position.

previous works (2.2% for $Zr_{60}Al_{10}Ni_{10}Cu_{20}$ metallic glass wire[19]) and seems to be over-estimated value. The Young's modulus listed in Table 3 was evaluated by the σ_f/l_f, although the accuracy is not high. But we can conclude that metallic glass wire shows extremely low Young's modulus compared with conventional metallic crystalline materials. And the low Young's modulus is suitable for biomaterials from the view point of removing the mismatch of Young's modulus between the human hard tissues and metallic implants.[36]

Average σ_f value of the Zr-Ti-Co alloy was under 1 GPa. The low σ_f compared with metallic glass single phase wire may be due to crystalline precipitates although the volume fraction of the precipitates is small. Figure 11 shows the typical example of surface ruggedness in melt extracted Zr-Ti-Co wire. Figure 11(a) shows that the wire shows a smooth surface and no distinct ruggedness, which is similar to Fig. 3(c) and (g). Figure 11(b) is the close-up image of the part indicated by the white arrow in Fig. 11(a). Surface ruggedness whose size is about 2 μm can be seen. This may reasons the origin of the fracture initiation during the tensile test, resulting in the decrease in σ_f. The precipitation of crystalline phase does not strongly affect the continuous wire

Table 3 Mechanical properties of melt-extracted Zr-based alloy wires.

Alloy-system	Alloy composition	(Alloy name)	σ_f [GPa]	ε_f [%]	E [GPa]
Zr-Nb-Al-Ni-Cu	$Zr_{57}Nb_5Al_{10}Ni_{12.6}Cu_{15.4}$	(Vit-106)	1.1	(2.7*)	
Zr-Ti-Al-Ni-Cu	$Zr_{52.5}Ti_5Al_{10}Ni_{14.6}Cu_{17.9}$	(Vit-105, BAM-11)	1.5	(3.2*)	
	$Zr_{55}Ti_{5.2}Al_{10.5}Ni_{13.2}Cu_{16.1}$		1.5	(2.7*)	
Zr-Ti-Al-Cu	$Zr_{52.5}Ti_5Al_{10}Cu_{32.5}$	(Ni free BAM-11)	1.6	(3.0*)	
Zr-Al-Co-Cu	$Zr_{65}Al_{7.5}Co_{10}Cu_{17.5}$		1.4	(2.9*)	(60**)
Zr-Al-Ni-Cu	$Zr_{65.0}Al_{7.5}Ni_{10}Cu_{17.5}$		1.8	(2.9*)	(71**)
Zr-Al-Co	$Zr_{65}Al_{7.5}Co_{27.5}$		1.1	(3.1*)	
Zr-Ti-Co	$Zr_{65}Ti_{7.5}Co_{27.5}$		0.77	(3.0*)	

(*): Elastic strain limit was evaluated not by strain gage but by the deviation of cross head. The accuracy of ε_f is not so high enough to discuss the absolute value because of the difficulty in chucking the wire.
(**): Young modulus E was evaluated by $\sigma_f/(\varepsilon_f^*0.01)$.

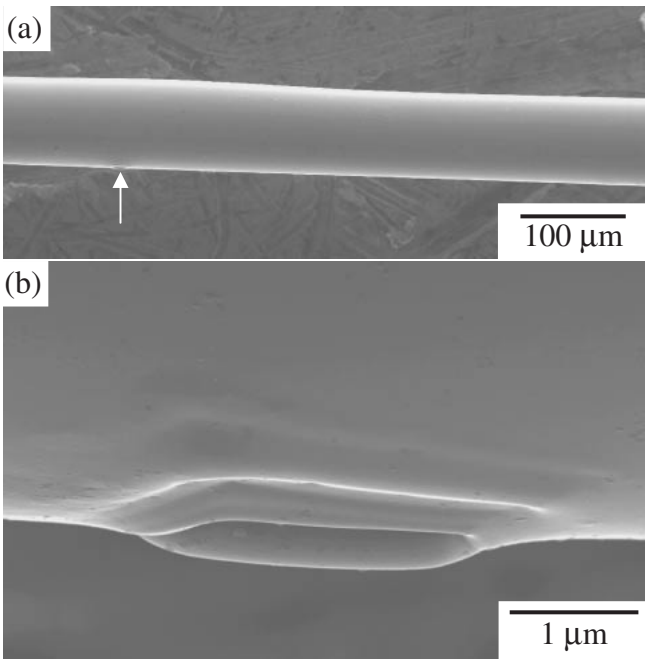

Fig. 11 SEM images of a defect in melt-extracted wires in $Zr_{65}Ti_{7.5}Co_{27.5}$ alloy with small amount of crystalline phase. (a) at low magnification and (b) at high magnification.

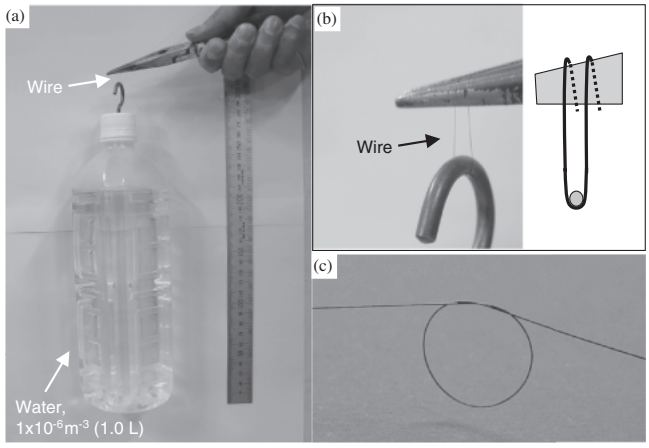

Fig. 12 Demonstration of high strength, ductility and easy handling in melt-extracted Zr-based metallic glass wires. (a) an example of lifting heavy load whose weight is about 1 Kg. (b) close-up image of (a) and (c) the knot of melt-extracted Zr-based metallic glass wire.

formation, amorphous structure and thermal properties, while the crystalline precipitates is very harmful to tensile fracture strength.

Figure 12 shows the demonstration of high tensile strength, ductility and easy handling in melt-extracted Zr-based metallic glass wires. Melt-extracted Zr-Al-Ni-Cu metallic glass wire did not fracture by lifting the load whose weight is about 1 Kg. It should be noticed that metallic glass wire can be bent through 180 degree without fracture in spite of heavy loading as shown in Fig. 12(b). The wire was not destroyed even if it was nipped by a pair of needle-nose pliers tightly. The superior ductility also can be confirmed by Fig. 12(c). Ductility of melt-extracted wire was evaluated by a simple bending test. All wires listed in Table 3 were bent through 180 degrees without fracture. The Zr-based metallic glass wires exhibit simultaneously high tensile strength, large elastic elongation, low Young's modulus and good bending ductility. The simultaneous achievement of high tensile strength, good bending ductility and high phase stability of an amorphous phase promises the melt-extracted Zr-based metallic glass wires for biomedical applications.

4. Discussion

In the present study, Zr-based metallic glass wires with high tensile fracture strength were obtained by arc-melting type melt-extraction method in spite of high reactivity of these molten states. The origin of higher cooling rate of the present process in comparison with that for the conventional melt-spinning method had been suggested in the previous study;[16,17] (1) the solidification from supercooled liquid without contact with other solid substrates leads to the suppression of heterogeneous nucleation of a crystalline phase, (2) the large ratio of outer surface area to volume enables the achievement of a high cooling rate, (3) the small volume enables the rapid cooling even by heat release to the Ar gas, and (4) the high flight velocity of the extracted wire in the Ar gas leading to the highly effective heat release due to the high velocity against Ar gas. These origins of higher cooling rate can be adapted in the present study.

In Zr-Al-Co and Zr-Ti-Co alloys, crystalline precipitates were seen in melt-extracted wire, while an amorphous single phase can be obtained in melt-spun ribbon. This difference can be explained by the difference in circumferential velocity of Cu roll. In melt-extraction method, the volume and ratio of outer surface area to the volume of extracted melt decreases with decreasing circumferential velocity. The lower the circumferential velocity of Cu roll is, the lower the cooling rate based on the above-described facts (2), (3) and (4) becomes. The cooling rate is very sensitive to the circumferential velocity of Cu roll. The difference in GFA between melt-extraction method and single roller melt-spinning method may be due to the difference in the circumferential velocity of Cu roll in the present study; 21 ms^{-1} (2000 r.p.m.) in melt-extraction method and 42 ms^{-1} (4000 r.p.m.) in single-roller melt-spinning method. In quinary Zr-Ti-Al-Ni-Cu alloys, quaternary Zr-Al-Ni-Cu, Zr-Al-Co-Cu and Zr-Ti-Al-Cu alloys, no significant difference in constituent phases and structure of an amorphous phase between melt-extraction method and conventional single-roller melt-spinning method was observed. Melt-extracted wire and melt-spun ribbon in these alloys show glass-to-supercooled liquid transition at the temperature T_g in DSC curves, while those in ternary alloys do not. The appearance of supercooled liquid region in DSC curves indicates extremely high phase stability of glassy phase against crystallization and high GFA. High thermal stability of an amorphous phase and high GFA in quinary and quaternary Zr-based alloys enable the formation of amorphous single phase by melt-extraction method.

Melt-extracted amorphous wires of 8 alloys listed in Table 2 show circular shape in cross section and the roundness over 95. The above-described cooling mechanism of melt-extraction process indicated that the cooling of liquid is mainly not due to the heat release through the contact with

other solid substrates such as Cu roll but through Ar atmosphere. The melt-extracted melt has an enough time to change the cross section shape from circle with concave to perfect circular shape. The unique cooling mechanism (1) mentioned above leads the formation of an amorphous wire with circular shape in cross section. The main cause of smooth surface without any ruggedness is due to little change in volume between liquid state and amorphous phase.

5. Conclusion

In the present study, the Zr-based metallic alloy wires for biomaterials were able to be prepared by arc-melting type melt-extraction method and their characteristics were studied, the following conclusions were reached:

(1) Metallic glass wires with large length over 1 m, little change in the diameter, good bending ductility and high fracture tensile stress over 1 GPa can be obtained not only in conventional Zr-based multi-component alloys but also Ni-free type alloys.

(2) In Ni and Al free Zr-Ti-Co alloy, metallic glass wire contains small quantity of crystalline precipitates. Continuous wires with good bending ductility can be obtained not only in an amorphous single phase alloy but also in the mixture of an amorphous phase and small amount of crystalline phases. The tensile fracture stress in Zr-based metallic wire is sensitive to the precipitation of crystalline phase.

(3) In $Zr_{60}Ti_{40}$ alloy, continuous metallic crystalline wire with good bending ductility can be obtained by melt extraction method.

(4) The melt-extraction technique is very effective for preparing Zr-based metallic amorphous and crystalline wires for biomaterials.

Acknowledgement

This work was supported by a Grant-in-Aid for Scientific Research on Priority Area A, “Materials Science of Metallic Glasses” from the Ministry of Education, Culture, Sports, Science and Technology of Japan. Part of this work was also supported by the same Ministry’s “Priority Assistance of the Formation of World-wide Renowned Centers of Research-The 21st Century COE Program (Project: Center of Excellence for Advanced Structural and Functional Materials Design)”.

REFERENCES

1) A. Inoue: Acta Mater. **48** (2000) 279–306.
2) A. Inoue: *Bulk Amorphous Alloys-Practical Characteristics and Applications, Materials Science Foundations 6*, (Trans Tech Publications, Switzerland, 1999).
3) M. Hagiwara, A. Inoue and T. Masumoto: Metall. Trans. A **13** (1981) 373–382.
4) M. Hagiwara, A. Inoue and T. Masumoto: Proc. 5th Inter. Conf. on Rapidly Quenched Metals, Ed. by S. Steeb and H. Warlimont, (Elsevier Sci Pub., Amsterdam, 1985) pp. 1779–1782.
5) A. Inoue, M. Hagiwara and T. Masumoto: J. Mater. Sci. **17** (1982) 580–588.
6) M. Hagiwara, A. Inoue and T. Masumoto: Mater. Sci. Eng. **54** (1982) 197–207.
7) K. Koshiba: Master thesis in Osaka university (1989).
8) A. Inoue, S. Furukawa, M. Hagiwara and T. Masumoto: Metall. Trans. A **18** (1987) 621–628.
9) T. Masumoto, I. Ohnaka, A. Inoue and M. Hagiwara: Scripta Mater. **15** (1981) 293–296.
10) A. Inoue, H. S. Chen, J. T. Krause, T. Masumoto and M. Hagiwara: J. Mater. Sci. **18** (1983) 2743–2751.
11) I. Ohnaka, T. Fukusako and T. Ohmichi: Production of Metal Filament by In-Rotating-Water Spinning Method, J. Jpn. Inst Met. **45** (1981) 751–758.
12) http://www.unitika.co.jp/shinki/MetallicFibers/bolfur.htm
13) http://www.unitika.co.jp/shinki/MetallicFibers/sency.htm
14) P. Rudkowski, G. Rudkowska and J. O. Strom-Olsen: Mater. Sci. Eng. A **133** (1991) 158–161.
15) J. O. Strom-olsen: Fine fibres by melt extraction, Mater. Sci. Eng. A **178** (1994) 239–243.
16) A. Inoue, A. Katsuya, K. Amiya and T. Masumoto: Mater. Trans., JIM **36** (1995) 802–809.
17) A. Inoue, K. Amiya, I. Yoshii, H. M. Kimura and T. Masumoto: Mater. Trans., JIM **35** (1994) 485–488.
18) A. Inoue, K. Amiya, A. Katsuya and T. Masumoto: Mater. Trans., JIM **35** (1995) 858–865.
19) H. Kimura, A. Inoue, K. Sasamori, H. Ohtsubo and Y. Waku: J. Jpn. Soc. of Powder and Powder Metallurgy **47** (1999) 427–432.
20) J. A. Tesk and C. E. Johnson: ASTM Spec. Tech. Publ. No. 1346 (1998) 69–75.
21) J. A. Tesk, C. E. Johnson, D. Skrtic, M. S. Tung and S. Hsu: ASTM Spec. Tech. Publ. No. 1365 (1999) 32–43.
22) H. Oonishi, E. Tsuji, T. Nabeshima, S. Kushitani, K. Tsuyama, Y. Ukon and N. Murata: Proc. of 6th European Conf. On Biomaterials, Bologna, Itary, September 14–17 (1986) 541–546.
23) S. Spriano and C. Antonione: Metall. Ital. **91** (1999) 63–69.
24) H. Nemoto, H. Katagiri, S. Meguro and K. Hashimoto: Proc. of Zairyo-to-Kankyo (2002) 253–254.
25) S. Hiromoto, H. Numata, A. P. Tsai, K. Nakazawa, T. Hanawa and H. Sumita: J. Japan Inst. Metals **63** (1999) 352–360.
26) S. Hiromoto: Kinou-Zairyo **22** (2002) 46–52.
27) E. Miura, H. Kato, T. Ogata, Y. Tanaka, T. Shiraishi, A. Inoue and K. Hisatsune: Proc. of BMG-IV, Tennessee (2005) 76.
28) S. Hiromoto, A. P. Tsai, H. Sumida and T. Hanawa: Collected Abstracts of the 2000 Spring Meeting of the Japan Inst. Metals (2000) 439.
29) J. J. Oak and A. Inoue: Mater. Sci. Eng. A **449–451** (2007) 220–224.
30) S. Buzzi, K. Jin, P. J. Uggowitzer, S. Tosatti, I. Gerber and J. F. Loffler: Intermetallics **14** (2006) 729–734.
31) J. A. Horton and D. E. Parsel: Mat. Res. Soc. Symp. Proc. **754** (2002) CC.1.5.
32) T. Cho and A. Inoue: Collected Abstracts of the 2002 Spring Meeting of the Japan Inst. Metals (2001) 279.
33) T. Wada, T. Cho and A. Inoue: Collected Abstracts of the 2002 Spring Meeting of the Japan Inst. Metals (2002) 349.
34) S. Hiromoto, A. P. Tsai, M. Sumita and T. Hanawa: Mater Trans. **42** (2001) 656–659.
35) S. Hiromoto, K. Asami, A. P. Tsai and T. Hanawa: Mater Trans. **43** (2002) 261–266.
36) J. A. Helsen and H. J. Breme: *Metals as biomaterials* (Wiley, Baffins Lane, Chichester, England, 1998).